Journal of Magnetic Resonance **157,** 52–60 (2002)
doi:10.1006/jmre.2002.2575

Quantifying the Lateral Lipid Domain Properties in Erythrocyte Ghost Membranes Using EPR-Spectra Decomposition

Zoran Arsov, Milan Schara, and Janez Štrancar

Laboratory of Biophysics, "Jožef Stefan" Institute, Jamova 39, 1000 Ljubljana, Slovenia

E-mail: zoran.arsov@ijs.si

Received December 27, 2001; revised May 21, 2002

Using EPR spectroscopy a typical lateral domain structure was detected in the membranes of spin-labeled bovine erythrocyte ghosts. The spectral parameters were determined by decomposing the EPR spectrum into three spectral components and tuned by a hybrid-evolutionary-optimization method. In our experiments the lateral domain structure and its properties were influenced by the variation in the temperature and by the addition of *n*-butanol. The specific responses of the particular domain types were detected. For the most-ordered domain type a break was seen in the temperature dependence of its order parameter, while the order parameters of the two less-ordered domain types exhibited a continuous decrease. Below the break-point temperature the alcohol-induced membrane fluidity variation is mainly a consequence of the change in the proportions of the least- and the most-ordered domain type and not the change of the domain-type ordering or dynamics (with *n*-butanol concentration). On the other hand, the fluidity variation above the break-point temperature arises from both types of changes. Interestingly, the proportion of the domain type that has its order parameter between that of the least- and the most-ordered domain type remains almost constant with concentration as well as with temperature, which implies its stability. Such characterization of the lateral membrane domain structure could be beneficial when considering the lipid–protein interactions, because it can be assumed that the activity of the membrane-bound enzyme depends on the properties of the particular domain type.

Key Words: **membrane fluidity; lateral lipid domain; membrane-bound enzyme activity; nitroxide spin probe; EPR spectroscopy.**

INTRODUCTION

Membrane fluidity, which is a characteristic of plasma membranes, is inversely related to membrane microviscosity (*1*). It reflects the ordering and dynamics of the phospholipid acyl chains in the membrane's bilayer. The organization of lipids in the membranes is described with the order parameter S, which represents the time-averaged angular fluctuation of the acyl chain segments from the normal to the bilayer plane (*2*); and by the rotational correlation time τ, which indicates the average time required for the molecular segments to forget their previous orientation (*3*). The fluidity of plasma membranes depends on their lipid and protein composition (*1*). It can be altered by external influences like the temperature or by the addition of compounds that interact with the membranes.

Biological membranes are laterally heterogeneous structures that can be effectively studied by electron paramagnetic resonance (EPR). A lateral membrane domain is usually considered to be a spatially limited region of a membrane that has one or more measurable properties that distinguish it from its neighboring regions (*4*). Motional parameters such as the rate and the anisotropy of motion of the spin label in a particular domain as well as the abundance of domains can be unambiguously determined by EPR; however, the size of domains and their shape cannot be derived from EPR spectra. Consequently, it is more appropriate to say that the properties of domain types can be determined using EPR. We will not deal with the question of how the domain structure arises, e.g., whether it is a consequence of lipid–lipid interactions or lipid–protein interactions (*5*). Also, we will not address the problem of the difference between the domain structure of the exoplasmic and the cytoplasmic membrane leaflets (*6*).

Using spin-labeled fatty-acid derivatives (spin probes) EPR allows us to characterize the fluidity of lipid phases (*7*). This fluidity is often described by empirical parameters of molecular ordering and dynamics, which can be derived directly from the positions and shapes of the spectral lines. But lately, with the upgrade to the heterogeneous picture of membrane structure, experimental approaches are able to provide a description of the local fluidity characteristics. Different experimental methods show the coexistence of domains; these methods include EPR, nuclear magnetic resonance, neutron diffraction, fluorescence methods, single-particle tracking, atomic force microscopy, and Raman spectroscopy (see reviews (*4, 5, 8*) and (*6, 9–13*)). The lateral lipid domains are thought to play an important role in some biological processes. That is why the understanding of the regulation of their formation, distance scale, and time scale (stability) is needed. Usually the formation of domains is the consequence of distinct molecular composition. Therefore, biological membranes are expected to exhibit heterogeneity at the molecular level because they have a large molecular diversity.

1090-7807/02 $35.00

So when a measurement indicates that a membrane region has distinctive properties, this implies that the measured properties are being averaged over a sufficiently long time to remove the intrinsic heterogeneities (*4*). This time is sufficient to observe the domains by a certain method, but it does not tell us more about the time scale of their stability. In addition, for domain sizes beyond the resolution of standard light microscopy techniques there is always an indirect evidence of their existence; usually lipid domains are defined through heterogeneities in the response of molecular probes.

EPR and its characteristic time scale for motional averaging 10^{-8} s, defined by the spin probe's nitroxide (spin Hamiltonian) interaction tensor anisotropy, seem to be appropriate because the lateral diffusion of the spin probe's molecules is too slow to average out the differences between the domains. On the other hand, under physiological conditions the rotational motions of molecules are fast. Consequently, we believe that the fast-motion approximation allows a sufficiently reasonable description of the spectra of fatty acid (methyl esters) spin probes in fluid biological membranes. The observed lateral membrane domain types are long-lived in comparison to the above-defined time scale. As a result, the heterogeneity of cell membranes results in spectra, which are a superimposition of several spectral components corresponding to particular domain types. Therefore, the EPR spectrum decomposition and the analysis of the spectral parameters allow the measurement of local fluidity characteristics, i.e., the order parameters and the rotational correlation times of each lipid domain type.

The activity of membrane-bound enzymes (e.g., see (*14–16*)) and the function of other membrane-bound supra-molecular structures have been described as depending on the membrane fluidity. As a consequence, if the fluidity varies in different domain types, we can assume that the activity of the enzyme molecules will depend on their position in the membrane. In order to be able to correlate the activity of an enzyme with the lateral membrane domain structure, it is necessary to measure the properties of particular domain types. Therefore, the aim of this work was a quantitative characterization of the lateral domain structure of the bovine erythrocyte ghost membrane using the method of EPR spectrum decomposition.

MATERIALS AND METHODS

Preparation of erythrocyte ghosts. The erythrocyte hematocrit was prepared by washing fresh bovine blood with a phosphate buffer solution (pH 7.4) three times; 12 ml of 50% hematocrit was chilled to 0°C and 120 ml of 4-mM $MgSO_4$ solution was added. The solution was stirred and left to mix for 5 minutes, all at 0°C. After that, 7 ml of 3.32-M NaCl was added. The solution was stirred and left to mix for 5 minutes, all at 0°C. The obtained mixture was incubated for approximately 50 minutes at 37°C and then cooled and centrifuged at 25,000 *g* for 15 minutes. The centrifugation (and washing with the buffer at the same time) was conducted three times.

Spin labeling. A total of 60 μl of 10^{-4}-M solution in ethanol of lipophilic spin probe, methyl ester of 5-doxyl palmitate MeFASL(10,3) (nitroxide radical), was added to the glass tube. The ethanol was evaporated so that the spin probe was uniformly distributed over the walls of the glass tube. After the final wash, the ghosts were suspended in a volume approximately three times larger than the volume of the membrane pellet. An appropriate volume of this suspension was added to the glass tube, so that the total volume (with the *n*-butanol added) of the sample was 750 μl. The tube was then shaken for 3 minutes. After that the labeled sample was centrifuged at 25,000 *g* for 5 minutes. The pellet was transferred into a glass capillary (1-mm inner diameter) and the EPR spectrum was recorded on a Bruker ESP 300 spectrometer (frequency 9.59 GHz, microwave power 20 mW). The spectra were accumulated in 2–4 scans with 167 s/scan in order to get a high signal-to-noise ratio. The ratio of the number of spin labels in the lipid phase to the number of lipid molecules was calculated to be approximately $N_{SL}/N_{lip} = 1/200$.

Contrasting the domain structure with n-butanol. In our experiments the fluidity variation of the erythrocyte ghost membranes was measured in the temperature range 295–320 K with a step of 2.5 K. In addition, *n*-butanol was used as a modifier of the membrane fluidity, which enabled us an additional access to vary the fluidity (*n*-butanol contrasting). This alcohol was chosen because it has a relatively high buffer-membrane partition coefficient (K) of 1.5 compared to its shorter-chained analogues (*17*) and as a result it has a larger effect on the membrane for a given concentration. In the control experiment no butanol was added; for 0.07, 0.15, 0.22, 0.37 M solutions of *n*-butanol 5, 10, 15, and 25 μl of *n*-butanol was added to the samples described above.

The EPR spectra decomposition and the determination of parameters. The recorded EPR spectra were characterized using spectrum simulation. The spectrum-simulation model was the so-called motional-restricted fast-motion approximation (*18*). In a membrane system, where molecular rotational motions are fast with respect to the EPR time scale, the magnetic interaction tensors can be averaged over the stochastic rotational motions of the spin probes. Subsequently, the spin Hamiltonian with averaged tensor components can be used to calculate lineshapes for the spin-probe molecules in membrane segments with their particular orientation relative to the external magnetic field. The spectra of the randomly oriented cell membrane segments are finally summed to get the inhomogeneously broadened spectra. Assuming the coexistence of long-lived lateral domains, we should expect that each spectrum is the superimposition of the spectral components that identify the membrane heterogeneity in the sample. The properties of the particular domain type are directly reflected in the values of the chosen parameter set. The set consists of order parameter S, effective rotational correlation time τ, additional broadening constant, hyperfine and Zeeman tensors' polarity correction factors, and weighting factors (proportions) w.

The software (EPRSIM Version 4.7; © Janez Štrancar) allows us to decompose a spectrum $I(B)$ into a different number of spectral components $I_i(B)$ related to the domain types with different order parameters and rotational correlation times in a magnetic field B (i is the domain-type index; w_i is the proportion so that $\sum_i w_i = 1$):

$$I(B) = \sum_i I_i(B)\, w_i. \qquad [1]$$

It should be stressed that an absolute measure of the domain-type proportion, which is proportional to the number of lipid molecules in a particular domain type $N_{lip,i}$, cannot be accurately determined. The reason is that the measured weighting factors w_i of the spectral components are proportional to the number of spin labels $N_{SL,i}$, and at the same time the ratio $(N_{lip}/N_{SL})_i$ can vary among the domain types. However, these ratios are assumed to be similar in different domain types since all domains are fluid, though with slightly different molecular ordering, in the relatively small temperature range that we studied. This implies that the proportions resemble the measured weighting factors w_i.

The parameters of the model were tuned by a hybrid-evolutionary-optimization procedure, which combines the deterministic simplex algorithm and the stochastic genetic algorithm (*19*). Before the optimization was started, the number of spectral components was chosen and the center field was adjusted. The maximum number of components that can be calculated with this software is 5, and we have chosen three ($i = 1, 2, 3$). One component was simulated to fit the outer hyperfine splitting ($i = 3$) and another one was matched with the most fluid domain type ($i = 1$). With only these two components it was not possible to obtain a satisfactory fit (according to our measurement of the goodness of fit χ^2, see below). In order to improve the fit a third component ($i = 2$), with its order parameter between that of domain types 1 and 3, was added (see Fig. 1).

For optimization purposes an objective function that measures the goodness of fit of the simulated spectrum to the experimental one had to be introduced. The measure is the reduced χ^2, i.e., the sum of the squared residuals between the experimental and the simulated spectra divided by the squared standard deviation of the experimental points, σ, and by the number of points in the experimental spectrum, N (in our case $N = 1024$):

$$\chi^2 = \frac{1}{N} \sum_{i=1}^{N} \frac{\left(y_i^{\exp} - y_i^{sim}\right)^2}{\sigma^2}. \qquad [2]$$

It should also be pointed out that the determination of the spectral parameter values should include an error estimation. In the simulation model the errors are calculated from diagonal elements of the covariance matrix and the correlation coefficients from the offdiagonal elements. Beside the χ^2 measure we also used eye matching between the measured and the calculated spectra as a criterion for accepting the best fit from a set of fits provided by multi-runs of the optimization.

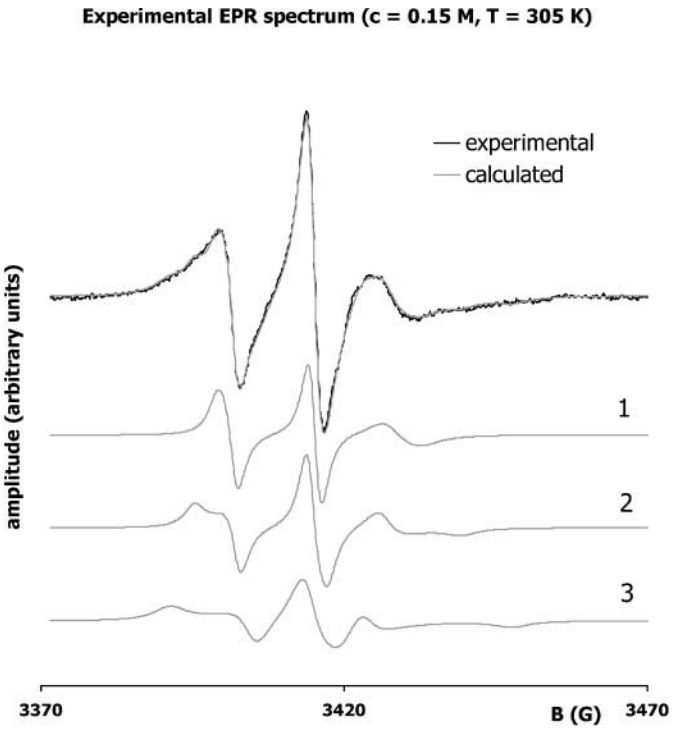

FIG. 1. Experimental EPR spectrum of the spin-labeled bovine erythrocyte ghost membrane (concentration of n-butanol 0.15 M, temperature 305 K) compared with the simulated spectrum. The simulated spectrum is decomposed into three spectral components ($i = 1, 2, 3$). The spectral parameters of a particular component are related to the properties of a particular domain type.

Three experiments were made and new erythrocyte ghosts were prepared each time. Five samples—a control and four different n-butanol concentrations—were measured at 11 temperatures in each experiment, so all together 165 spectra were recorded. To get the best possible fit the optimization of the same spectrum was done 6 times. It took approximately 400 h of CPU time to conduct these 990 optimizations on a dual-processor (933 MHz Intel Pentium III) PC. Each spectrum was optimized only 6 times because the optimization is time consuming. The problem is computationally demanding because the number of model parameters is usually high and nonlinear relations are involved. In our experience, the probability of getting a better fit by using more optimizations is no higher than 10–20%, and so an appropriate balance needs to be found between the number of optimizations and the time required. It is also worth remembering that the probability of finding the real global minimum is very high due to the use of the stochastic genetic algorithm. The best-fitted spectrum-simulation parameters were used to draw the plots presented under Results.

RESULTS

Figures 2–4 show the temperature dependence of the particular domain type i order parameter S_i, rotational correlation time

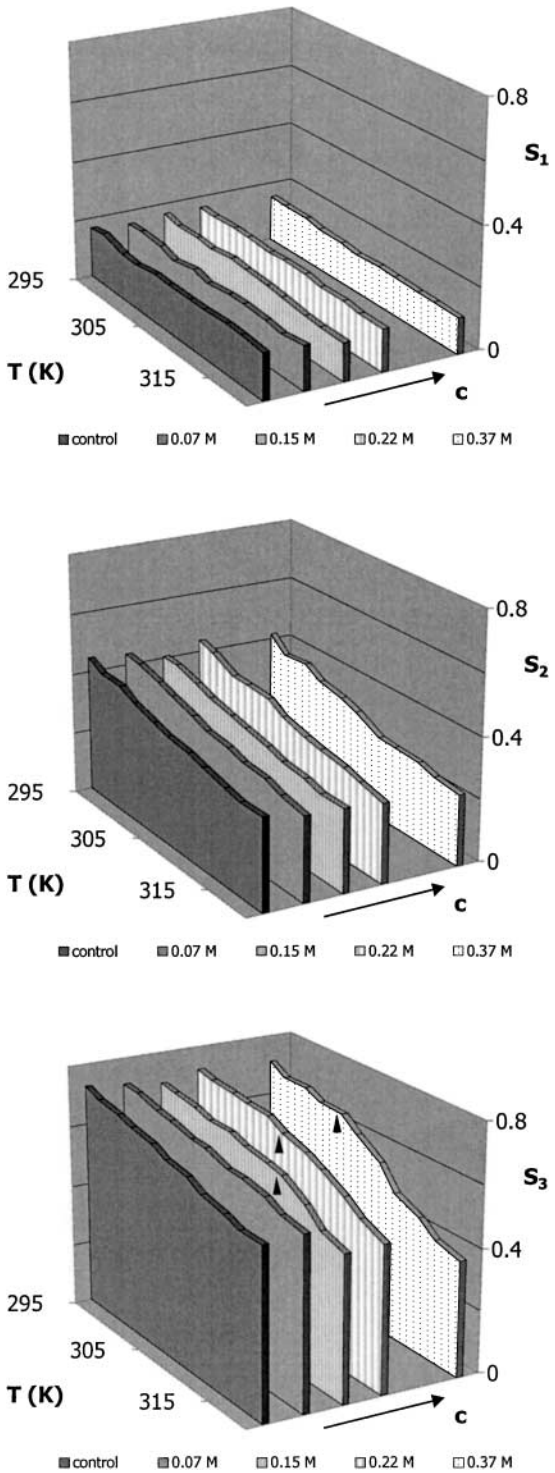

FIG. 2. The temperature dependence of the order parameter S_i for a particular domain type $i = 1, 2, 3$, displayed for different n-butanol concentrations (each point represents the average value of three different experiments). The arrows indicate the breaks where the slope $(\partial S_3/\partial T)_c$ changes abruptly. The temperatures T^* at these points are presented in Fig. 5.

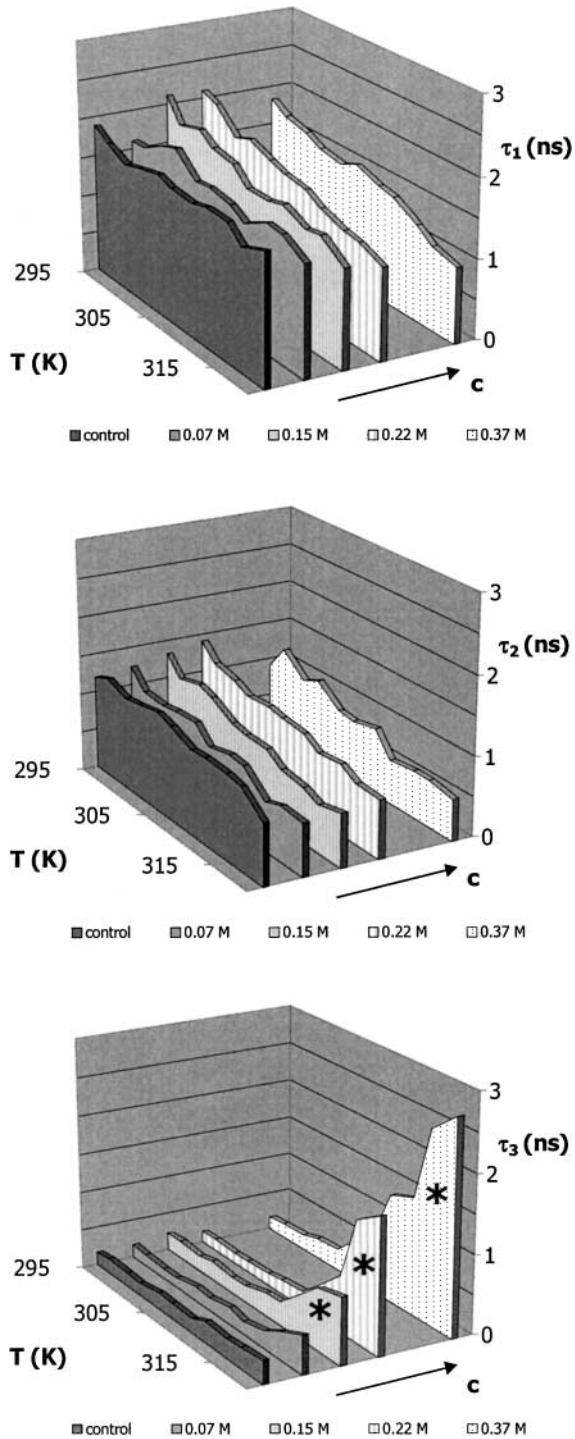

FIG. 3. The temperature dependence of the rotational correlation time τ_i for a particular domain type $i = 1, 2, 3$, displayed for different n-butanol concentrations (each point represents the average value of three different experiments). The asterisks in the graph of τ_3 indicate the ambiguity of the increase of τ_3 with T (see under Discussion for explanation).

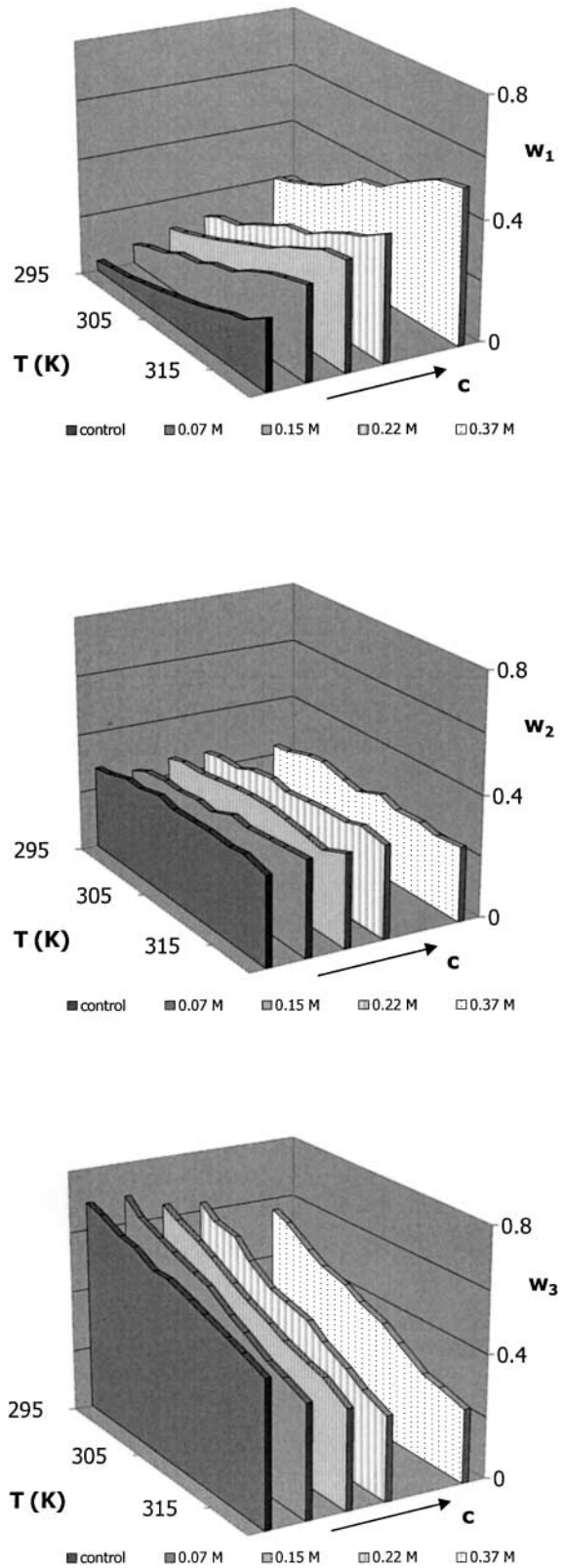

FIG. 4. The temperature dependence of the proportion w_i for a particular domain type $i = 1, 2, 3$, displayed for different n-butanol concentrations (each point represents the average value of three different experiments).

τ_i, and proportion w_i for different n-butanol concentrations c. The slopes $(\partial S_i/\partial T)_c$ and $(\partial w_i/\partial T)_c$ for the particular domain type relating to the different alcohol concentrations are summarized in Table 2. In Fig. 5 the concentration dependence of the characteristic temperature T^*, at which the break in the temperature dependence of S_3 occurs, is presented.

There is no significant difference between the values of the order parameters S_1, S_2 (and similarly, the rotational correlation times τ_1, τ_2) of the two less-ordered domain types when the alcohol concentration is increased (Figs. 2 and 3). Similar behavior is also seen for the parameters of the most-ordered domain type below the break-point temperature T^*. In other words, below T^* the values of the order parameter S_3 and the rotation correlation time τ_3 are similar for all the samples, independent of the alcohol concentration (see Figs. 2 and 3). High fluctuations in the graphs for rotational correlation times (Fig. 3) are a consequence of high errors on these parameters, e.g., for the control sample the order of size of the errors is ± 0.6, ± 0.2, and ± 0.1 ns for τ_1, τ_2, and τ_3, respectively. In contrast, the proportions of the most- (w_3) and the least-ordered domain type (w_1) are modified significantly by n-butanol, even below T^*. The proportion of the least-ordered domain type w_1 increases with concentration, whereas w_3 decreases (Fig. 4). However, the proportion w_2 of domain type 2 does not change significantly, either with concentration or temperature (Fig. 4).

The credibility of these important results was examined with an additional numerical experiment, which should confirm that below T^* the domain-type order parameters do not change significantly with alcohol concentration but the proportions, except for w_2, do. Therefore, optimized spectra of a sample containing n-butanol were taken and fitted once again by the simplex algorithm, with the starting set of parameters taken from optimized control spectra with no n-butanol added, so that: (A) the domain-type order parameters were fixed and could not change during the optimization, and (B) the proportions were fixed and could not change during optimization. An example of this procedure on a randomly chosen experimental spectrum where the concentration of n-butanol was 0.22 M is shown in Table 1. The values of χ^2 are much lower in the case of the fixed domain-type order parameters (Table 1A) for almost all temperatures, which indicates that our assumption is correct.

In the temperature range covered by our experiments an abrupt change in the slope of the temperature dependence of S_i occurred only in the most-ordered domain type, while the other

TABLE 1

The Goodness of Fit χ^2 Given by the Simplex Optimization of a Spectrum of a Sample with Added n-Butanol: (A) Fixed S_i, (B) Fixed w_i

	T (K)	295	297.5	300	302.5	305	307.5	310	312.5	315	317.5	320
A	χ^2	5.6	7.1	6.9	8.4	14.0	8.4	22.4	10.2	20.2	22.6	13.4
B	χ^2	8.8	11.7	24.0	16.1	24.6	11.9	23.8	17.6	17.7	27.9	15.7

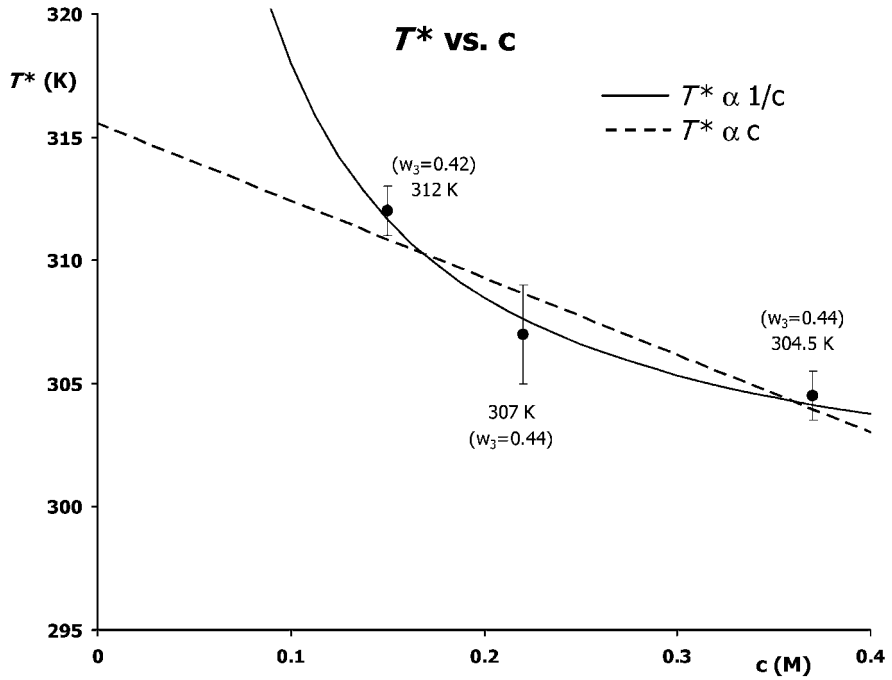

FIG. 5. The effect of different n-butanol concentrations on the temperatures T^* of the break-point in the slope $(\partial S_3/\partial T)_c$ seen in Fig. 2 (points and bars represent the mean ±S.D. from three different experiments). The proportion of the most-ordered domain type w_3 at these points was always around 0.43 as indicated on the graph (see parentheses). Since no breaks were seen for the control sample and for the sample with a 0.07-M n-butanol concentration, a nonlinear function $T^*(c)$ was supposed (full line on the graph; the dependence was fitted as $T^* \propto 1/c$). For comparison, see also a linear fit (dashed line).

two domain types showed a moderate linear decrease in the order parameters with temperature. The broken linear temperature dependence of the order parameter of the most-ordered domain type was fitted by the method of least squares. The breaks were clearly seen for three n-butanol concentrations 0.15, 0.22, and 0.37 M, and the characteristic temperatures T^* of these breaks were approximately 312, 307, and 304.5 K, respectively (indicated by the arrows in Fig. 2). The dependence of T^* on the concentration c is presented in Fig. 5. Since the breaks were not observed for the lowest alcohol concentration and for the control sample in the examined temperature interval, the dependence is expected to be nonlinear (see Fig. 5).

TABLE 2

Comparison of the Slopes of the Temperature-Dependence Plots of S_i and w_i for Different n-Butanol Concentrations for Domain Types $i = 1, 2, 3$

Domain type i	c (M)	$(\frac{\partial S_i}{\partial T})_c$ (10^{-3} K^{-1})		$(\frac{\partial w_i}{\partial T})_c$ (10^{-3} K^{-1})
1	0	-0.3 ± 0.3		$+7.7 \pm 0.5$
	0.07	-0.6 ± 0.3		$+10.1 \pm 0.3$
	0.15	-1.5 ± 0.3		$+11.5 \pm 0.3$
	0.22	-1.0 ± 0.2		$+12.0 \pm 0.4$
	0.37	-1.4 ± 0.1		$+13.3 \pm 0.7$
2	0	-6.2 ± 0.3		$+0.9 \pm 0.5$
	0.07	-6.7 ± 0.2		$+0.3 \pm 0.3$
	0.15	-6.0 ± 0.3		$+1.0 \pm 0.5$
	0.22	-7.0 ± 0.3		$+2.2 \pm 0.4$
	0.37	-7.3 ± 0.5		0 ± 0.7
		Below T^*	Above T^*	
3	0	-7.5 ± 0.2	/	-8.5 ± 0.3
	0.07	-6.2 ± 0.3	/	-12.7 ± 0.4
	0.15	-5.5 ± 0.4	-18 ± 2	-12.6 ± 0.3
	0.22	-4.3 ± 0.6	-15 ± 1	-14.2 ± 0.4
	0.37	-7 ± 1	-18 ± 1	-13.3 ± 0.4

Note. Data are presented as a value of slope ±S.E.

The results for τ_3 shown in Fig. 3 imply that τ_3 increases with T above T^* and for the highest three butanol concentrations. As it will be discussed in the next section the increase is questionable and the asterisks in Fig. 3 indicate this.

The slopes of the linear fits to the temperature dependence of the domain-type order parameters and the temperature dependence of the proportions for the particular domain type are presented in Table 2. The small alteration in S_1 and w_2 with temperature seen in Figs. 2 and 4, respectively, is reflected in Table 2 by the small slopes $(\partial S_1/\partial T)_c$ and $(\partial w_2/\partial T)_c$. It is clear from Table 2 that the slopes $(\partial S_3/\partial T)_c$ determined for the different alcohol concentrations change considerably above and below T^*. When the slopes for the proportions are compared, a jump in the value of $(\partial w_{1,3}/\partial T)_c$ is seen between the control sample and the samples with the higher alcohol concentrations.

DISCUSSION

As a consequence of the presence of the different molecular species in biological membranes, phase separation can occur

(*20, 21*). The resulting lateral membrane heterogeneity was also observed in our experiments on bovine erythrocyte ghosts using EPR-spectra decomposition. Since ghosts enable an accurate spectrophotometric assay of enzyme activity, they were used instead of intact erythrocytes. Since the membrane-bound enzyme activity may depend on the properties of the particular domain type, the overall activity A can be calculated as a weighted sum of the effective enzyme activities A_i in the corresponding particular domain type. Supposing an inhomogeneous distribution of the enzyme molecules (*22*) in the particular domain types the overall enzyme activity can be written as

$$A = \sum_i \frac{N_{enz,i}}{N_{enz,total}} A_i(S_i, \tau_i), \qquad [3]$$

where $N_{enz,i}$ is the number of enzyme molecules in domain type i and $N_{enz,total} = \sum_i N_{enz,i}$ is the total number of enzyme molecules. In addition, if the enzyme molecules were to be homogeneously distributed over the membrane, we could infer that $(N_{enz,i}/N_{enz,total}) \propto w_i$. In order to determine A_i, the properties of each domain type should be characterized in terms of its order parameter S_i, rotational correlation time τ_i, and proportion w_i.

In order to gain a deeper insight into the domain structure of the erythrocyte ghost membrane we varied the n-butanol concentration (as well as the temperature). The addition of alcohol did not influence the temperature dependence of the order parameters of the two less-ordered domain types (Fig. 2). Only a continuous decrease of the lipid ordering with temperature was observed, which means that the acyl chain conformational and motional freedom is continuously increasing with higher temperatures. In contrast, for the most-ordered domain type ($i = 3$) a break in the slope of the temperature dependence of S_3 can be observed at the characteristic temperature T^* (Fig. 5). The break, i.e., T^*, is shifted to lower temperatures when the concentration of n-butanol is increased (Fig. 5).

Similarly, the alcohol does not affect the temperature dependence of the rotational correlation time of the two fluid-domain types (Fig. 3), but τ_3 seems to increase at higher alcohol concentrations and above T^* (Fig. 3). The negative $(\partial\tau_{1,2}/\partial T)_c$ (see Fig. 3) is expected if the system does not change dramatically with T (*3*). Since τ_3 shows increase with T, this unexpected temperature dependence was examined with another numerical experiment. An optimized spectrum of a sample containing n-butanol was taken and was fitted once again by the simplex algorithm, where the starting set of parameters were parameters obtained from the hybrid-evolutionary optimization except for the value of τ_3, which was fixed. The value, to which it was fixed, was an average for the control sample of the same experiment. The comparison of the goodness of fit for the experimental spectra of a randomly chosen sample (concentration of n-butanol was 0.37 M) is shown in Table 3: (A) the original value of the goodness of fit and (B) the value of the goodness of fit after the simplex optimization with fixed τ_3. Table 3 shows that the differences between the values of χ^2 between case (A) and (B) are small. In addition, the values of other parameters did not change significantly in the second case (data not shown). These two observations imply that it is not straightforward to conclude that τ_3 should increase with temperature at higher alcohol concentrations and above T^*. Due to the ambiguity of the temperature dependence of τ_3, it would be challenging to inspect it with a different spectrum-simulation model or a different experiment.

TABLE 3

The Goodness of Fit χ^2 after: (A) The Original Hybrid-Evolutionary Optimization of a Spectrum of a Sample with Added *n*-Butanol, (B) The Additional Simplex Optimization with Fixed τ_3 (=0.17 ns)

	T (K)	295	297.5	300	302.5	305	307.5	310	312.5	315	317.5	320
A	χ^2	5.6	7.5	5.8	4.9	7.2	4.8	7.7	8.9	9.4	9.3	11.4
B	χ^2	5.8	7.6	5.8	4.8	7.3	4.6	8.3	9.8	8.8	10.9	11.6

It can be seen that at temperatures below T^* the influence of alcohol on the membrane fluidity is expressed only in the change of proportions (Fig. 4), whereas above T^* both the proportions (Fig. 4) as well as S_3 (Fig. 2)—and probably also τ_3 (Fig. 3)—change with alcohol concentration. Consequently, it can be concluded that the incorporation of n-butanol molecules into the most-ordered domain type becomes less restricted at a specific temperature, which we have denoted as T^*. The restriction below T^* could be due to a high S_3 (*23*). This might be explained by the higher partitioning of cholesterol molecules in ordered lipid domains, which can expel alcohol molecules (*24*). On the other hand, less restricted incorporation above T^* might be induced by the conformational reorganization of the most-ordered domain type. It is also possible that a phase transition occurs at T^*. Whatever the explanation, the abrupt increase in the absolute value of the slope $(\partial S_3/\partial T)_c$ above T^* (see Table 2) and the (dubious) increase of τ_3 with temperature at higher alcohol concentrations and above T^* (Fig. 3) seems to be conditioned by the more intense incorporation of n-butanol molecules.

The slopes $(\partial S_3/\partial T)_c$ for different concentrations below T^* are similar (see Table 2) since the partitioning of the n-butanol molecules is low. Surprisingly, the slopes $(\partial S_3/\partial T)_c$ are also similar above T^* (Table 2). One possible explanation is that at total n-butanol concentrations of 0.15, 0.22, and 0.37 M the membrane concentration of alcohol in the domain type 3 is approaching its saturation concentration (*25*). This assumption is supported by the fact that the ratio of n-butanol to lipid molecules N_{but}/N_{lip} can be quite high for the concentrations used. It can be calculated from the partition coefficient that this ratio $(N_{but}/N_{lip}) \approx 1/2$ for a 0.37-M concentration. Furthermore, the observation that for lower alcohol concentrations the slope $(\partial w_{1,3}/\partial T)_c$ changes faster than for higher concentrations (Table 2) also supports the idea of saturation.

The decrease of T^* with n-butanol concentration (Fig. 5) could be explained in terms of alcohol acting as an impurity in the mixture and thus lowering the phase transition temperature

(*26*). Although the discontinuities in the EPR spectral parameters measured on the spin-labeled erythrocyte ghosts have already been related to phase transitions (*27, 28*), some attention must be paid to such relations (*29*). An alternative explanation comes from the observation that the proportion of the most-ordered domain type w_3 is always similar (around 0.43) at T^* (see Fig. 5). This suggests that the value of w_3 plays a role in providing the condition for the break. Since w_3 reaches this value at a lower temperature for a higher alcohol concentration, the T^* concentration dependence can be explained. The suggested importance of the value of w_3 points to the possibility that the connectivity threshold (percolation) of the domain structure might appear at T^* (*30*). In addition, the threshold can directly influence the exchange of lipid and alcohol molecules, which could help in the explanation of the observed changed affinity of the domain type 3 for the *n*-butanol molecules above and below T^*. However, it should be stressed that the percolation cannot be predicted from the absolute value of w_3 (*31*). Another explanation for the decrease of T^* with *n*-butanol concentration follows from the assumed nonlinear concentration dependence of T^* (Fig. 5), which could be a consequence of the saturation discussed in the previous paragraph.

In the above discussion we dealt with the observed reorganization of the most-ordered domain type exposed to higher *n*-butanol concentrations. We also showed that the observed properties of the two less-ordered domain types do not depend on the *n*-butanol concentration.

Now we turn to the discussion about the characteristic properties of the domain type 2. Since its lipid ordering qualifies it to be in between those of the domain types 1 and 3 (Fig. 2), it could be assumed that domains of type 2 are located in between the least- and the most-ordered domain type. In this model there is no direct contact between the domains of types 1 and 3. On the other hand, the domains of type 2 can be a self-consistent part of a membrane, and in this model the domains of types 1 and 3 are in direct contact. Such a situation is also supported by the fact that the proportion w_3 decreases at the expense of w_1 with concentration and at the same time the proportion w_2 remains almost constant with concentration (Fig. 4). The decrease in the proportion w_3 at the expense of w_1 is due to the gradual partial change of the domains' 3 boundaries into a phase akin to the domain type 1. This is facilitated by lipid exchange in the boundary regions. In contrast, since w_2 remains almost constant, we would expect the phospholipid molecules in the domains of type 3, close to the boundary between the domains of types 3 and 2, not to perturb the contacting phases. It appears, therefore, that the domain type 2 is somehow stabilized. The special properties of the domain type 2 have been suggested before (*6*), where the stability of the domain type 2 was explained by its specific phospholipid composition. Another possibility could be that the domains contributing to the domain type 2 are associated with some of the erythrocytes' supra-molecular structure, like embedded proteins. It is believed that domains defined by such structures could be relatively stable (*32*).

CONCLUSIONS

We used the method of EPR-spectra decomposition to characterize the bovine erythrocyte ghost membrane lateral domain structure. The domain-type order parameters, the domain-type rotational correlation times, and the domain-type proportions were quantified by optimizing the simulated spectrum with a hybrid-evolutionary-optimization method. At physiologically relevant temperatures we believe that the fast-motion approach satisfactorily describes the EPR spectra and that reliable data can be obtained by the application of the optimization method. In the temperature range covered by our experiments the break in the temperature dependence of the order parameter occurred only in the most-ordered domain type, while in the two more-fluid domain types only a continuous and moderate decrease of the lipid ordering was observed. The alcohol-induced membrane fluidity variation below the break is mainly a consequence of the change in the proportions of the least- and the most-ordered domain type with *n*-butanol concentration. Interestingly, the proportion of the domain type, which has its ordering between the ordering of the least- and the most-ordered domain type, remains almost constant with concentration as well as with temperature, which implies its stability. On the other hand, the fluidity change above the break-point temperature also arises from changes in the domain-type ordering and dynamics. It can be concluded that the effect of *n*-butanol molecules is selective in terms of its effect on the motional characteristics of lipid molecules in different domain types. Such selectivity and its effect on the domain-type properties might be helpful in an investigation of the lipid–protein interactions in the membrane because it is believed that the membrane-bound enzyme activity depends on local fluidity characteristics.

ACKNOWLEDGMENT

This work was carried out with the financial support of the Ministry of Education, Science, and Sport of the Republic of Slovenia.

REFERENCES

1. M. Shinitzky, Membrane fluidity and cellular functions, *in* "Physiology of Membrane Fluidity" (M. Shinitzky, Ed.), Vol. 1, pp. 1–51, CRC Press, Boca Raton (1984).
2. W. L. Hubbell and H. M. McConnell, Molecular motion in spin-labeled phospholipids and membranes, *J. Am. Chem. Soc.* **93,** 314–326 (1971).
3. J. H. Freed, Theory of slow tumbling ESR spectra for nitroxides, *in* "Spin Labeling, Theory and Applications" (L. J. Berliner, Ed.), pp. 53–132, Academic Press, New York (1976).
4. M. Bloom and J. L. Thewalt, Time and distance scales of membrane domain organization, *Mol. Membr. Biol.* **12,** 9–13 (1995).
5. R. Welti and M. Glaser, Lipid domains in model and biological membranes, *Chem. Phys. Lipids* **73,** 121–137 (1994).
6. M. Žuvič-Butorac, P. Müller, T. Pomorski, J. Libera, A. Herrmann, and M. Schara, Lipid domains in the exoplasmic and cytoplasmic leaflet of the erythrocyte membrane: A spin label approach, *Eur. Biophys. J.* **28,** 302–311 (1999).

7. D. Marsh, Electron spin resonance: Spin labels, *in* "Membrane Spectroscopy" (E. Grell, Ed.), pp. 51–142, Springer-Verlag, Berlin (1981).
8. M. Edidin, Lipid microdomains in cell surface membranes, *Curr. Opin. Struct. Biol.* **7,** 528–532 (1997).
9. W. Rodgers and M. Glaser, Characterization of lipid domains in erythrocyte membranes, *Proc. Natl. Acad. Sci. USA* **88,** 1364–1368 (1991).
10. L. M. S. Loura, A. Fedorov, and M. Prieto, Fluid-fluid membrane microheterogeneity: A fluorescence resonance energy transfer study, *Biophys. J.* **80,** 776–788 (2001).
11. M. Tomishige and A. Kusumi, Compartmentalization of the erythrocyte membrane by the membrane skeleton: Intercompartmental hop diffusion of band 3, *Mol. Biol. Cell* **10,** 2475–2479 (1999).
12. H. A. Rinia and B. de Kruijff, Imaging domains in model membranes with atomic force microscopy, *FEBS Lett.* **504,** 194–199 (2001).
13. A. Percot and M. Lafleur, Direct observation of domains in model stratum corneum lipid mixtures by raman microspectroscopy, *Biophys. J.* **81,** 2144–2153 (2001).
14. T. C. Squier, D. J. Bigelow, and D. D. Thomas, Lipid fluidity directly modulates the overall protein rotational mobility of the Ca-ATPase in sarcoplasmic reticulum, *J. Biol. Chem.* **263,** 9178–9186 (1988).
15. L. M. Gordon, R. D. Sauerheber, J. A. Esgate, I. Dipple, R. J. Marchmont, and M. D. Houslay, The increase in bilayer fluidity of rat liver plasma membranes achieved by the local anaesthetic benzyl alcohol affects the activity of intrinsic membrane enzymes, *J. Biol. Chem.* **255,** 4519–4527 (1980).
16. A. Spinedi, P. Luly, and R. N. Farias, Does the fluidity of the lipid environment modulate membrane-bound acetylcholinesterase? *Biochem. Pharmacol.* **46,** 1521–1527 (1993).
17. P. Seeman, The membrane actions of anesthetics and tranquilizers, *Pharmacol. Rev.* **24,** 583–655 (1972).
18. J. Štrancar, M. Šentjurc, and M. Schara, Fast and accurate characterization of biological membranes by EPR spectral simulations of nitroxides, *J. Magn. Reson.* **142,** 254–265 (2000).
19. B. Filipič and J. Štrancar, Tuning EPR spectral parameters with a genetic algorithm, *Appl. Soft Comput.* **1,** 83–90 (2001).
20. E. J. Shimshick and H. M. McConnell, Lateral phase separation in phospholipid membranes, *Biochemistry* **12,** 2351–2360 (1973).
21. O. G. Mouritsen and K. Jørgensen, Dynamical order and disorder in lipid bilayers, *Chem. Phys. Lipids* **73,** 3–25 (1994).
22. E. C. C. Melo, I. M. G. Lourtie, M. B. Sankaram, T. E. Thompson, and W. L. C. Vaz, Effects of domain connection and disconnection on the yields of in-plane bimolecular reactions in membranes, *Biophys. J.* **63,** 1506–1512 (1992).
23. M. K. Jain, J. Gleeson, A. Upreti, and G. C. Upreti, Intrinsic perturbing abilitiy of alkanols in lipid bilayers, *Biochim. Biophys. Acta* **509,** 1–8 (1978).
24. O. G. Mouritsen and K. Jørgensen, Micro-, nano- and meso-scale heterogeneity of lipid bilayers and its influence on macroscopic membrane properties, *Mol. Membr. Biol.* **12,** 15–20 (1995).
25. M. J. Pringle, K. B. Brown, and K. W. Miller, Can the lipid theories of anesthesia account for the cutoff in anesthetic potency in homologous series of alcohols? *Mol. Pharmacol.* **19,** 49–55 (1981).
26. M. W. Hill, The effect of anaesthetic-like molecules on the phase transition in smectic mesophases of dipalmitoyllecithin. I. The normal alcohol up to C = 9 and three inhalation anaesthetics, *Biochim. Biophys. Acta* **356,** 117–124 (1974).
27. T. Ogiso, M. Iwaki, and K. Mori, Fluidity of human erythrocyte membrane and effect of chlorpromazine on fluidity and phase separation of membrane, *Biochim. Biophys. Acta* **649,** 325–335 (1981).
28. L. M. Gordon and P. W. Mobley, Thermotropic lipid phase separations in human erythrocyte ghosts and cholesterol-enriched rat liver plasma membranes, *J. Membr. Biol.* **79,** 75–86 (1984).
29. P. F. Devaux and M. Seigneuret, Specificity of lipid-protein interactions as determined by spectroscopic techniques, *Biochim. Biophys. Acta* **822,** 63–125 (1985).
30. M. B. Sankaram, D. Marsh, and T. E. Thompson, Determination of fluid and gel domain sizes in two-component two-phase lipid bilayers: An electron spin resonance spin label study, *Biophys. J.* **63,** 340–349 (1992).
31. W. L. C. Vaz, E. C. C. Melo, and T. E. Thompson, Translational diffusion and fluid domain connectivity in a two-component, two-phase phospholipid bilayer, *Biophys. J.* **56,** 869–876 (1992).
32. J.-F. Tocanne, L. Cezanne, A. Lopez, B. Piknova, V. Schram, J.-F. Tournier, and M. Welby, Lipid domains and lipid-protein interactions in biological membranes, *Chem. Phys. Lipids* **73,** 139–158 (1994).